Journal of Magnetic Resonance **140,** 285–288 (1999)
Article ID jmre.1999.1846, available online at http://www.idealibrary.com on IDEAL®

Target Field Design for Magic Angle Gradient Coils

Thomas M. Barbara and Charles E. Bronnimann

Varian NMR Instruments, 3120 Hansen Way, Palo Alto, California 94303

Received March 31, 1999; revised June 16, 1999

The target field method of designing gradient coils is extended to the case where the gradient producing currents lie on cylinders of a general orientation with respect to the polarizing magnetic field. This provides a general approach for designing coils that require unusual sample geometries such as those required for magic angle spinning (MAS) applications. A detailed example of a magic angle gradient coil set for MAS is given. © 1999 Academic Press

Key Words: **magic angle gradients; target field method; gradient design; magic angle spinning.**

The current interest in magic angle gradient coils originated from applications involving water suppression in DQF-COSY (*1*) and the use of MAS to obtain high-resolution spectra from small sample volumes (*2*) or heterogeneous liquid environments (*3*). Magic angle gradient coils for water suppression employ the standard high-resolution sample geometry where the sample axis is along the polarizing magnetic field direction and the gradient currents are wound on cylindrical formers coaxial with both. Such gradients can be produced by superimposing standard Z gradient coils with transverse X or Y gradients, or they can be designed using an integrated winding pattern determined by target fields as proposed by Bowtell and Peters (*4*). The same type of design can in principle be used for MAS experiments where the sample and rotation axis are at the magic angle with respect to the polarizing field. This approach however suffers from poor efficiency and precludes easy sample access. The alternative of winding a Maxwell pair around the sample will also be inefficient since only the projection of the gradient field along the polarizing field will contribute. For the same reason, large spinning modulation effects will arise from the radial component of the magnetic field produced by the coil.

A solution to these shortcomings was proposed by Cory and co-workers, where the gradient coil, aligned along the sample axis, is designed from the outset to have small modulation components as well as a gradient along the coil former axis (*5*). The purpose of this Communication is to show how the target field method, widely used in the design of standard gradient coils (*6*), can be extended to coils for MAS gradient applications.

The magic angle gradient coil geometries for standard high-resolution and MAS applications are illustrated in Fig. 1, where the vector $\mathbf{K}$ denotes the direction of the gradient, and $\mathbf{B}_0$ the main polarizing field. Currents that produce the gradient field are constrained to lie on the surface of the cylinders, and one method used to derive the shape of the currents is by way of the boundary conditions for magnetic fields and surface currents (*7*). In this approach, the component of the gradient field is assigned a linear variation in the desired direction. Additional terms are then added to the gradient magnetic field so that the total field possesses zero divergence and curl, as required by Maxwell's equations. Once a consistent gradient field is specified, the surface current $\mathbf{J}$ producing such a field is given by

$$\mu_0 \mathbf{J} = \mathbf{e}_\rho \times \mathbf{B}, \qquad [1]$$

where $\mathbf{e}_\rho$ is the outward-directed unit vector normal to the cylinder. For case (A) in Fig. 1, the desired gradient field variation, $G(\mathbf{K} \cdot \mathbf{r})e_z$, with the $\mathbf{K}$ vector components (0, sin θ, cos θ), must be augmented with a term along the y axis, so that the total field is

$$\mathbf{B}_A(\theta) = G(z \cos\theta + y \sin\theta)\mathbf{e}_z + G(z \sin\theta - y \cos\theta)\mathbf{e}_y. \qquad [2]$$

Similarly, the augmented field for MAS gradient design in Fig. 1B yields a total field $\mathbf{B}_B(\theta) = \mathbf{B}_A(-\theta)$. The current densities obtained for both types of coils by applying Eq.[1] are therefore closely related to each other. Wire patterns that approximate the desired current densities can be obtained from the contours of the scalar stream function (*4*), after suitable truncation that forces the current density to zero outside some finite length along the cylinder axis. This procedure will produce additional terms to the original current density in order to satisfy conservation of charge. Let $F(z)$ represent a general truncating function which goes to zero outside some chosen region about $z = 0$, but is almost constant within that region. Then the general form for the stream function in cylindrical coordinates ρ, ϕ, z for a MAS gradient coil will be

1090-7807/99 $30.00

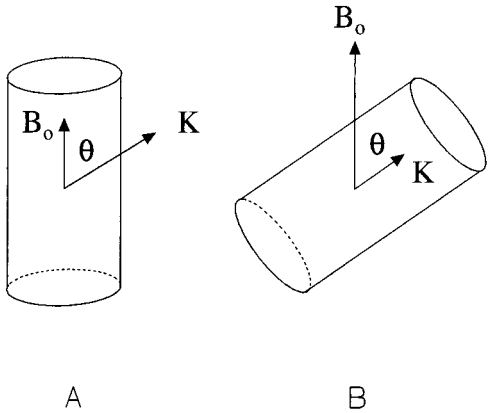

FIG. 1. Magic angle gradient coil geometries for normal high-resolution sample geometry (A) and for samples spinning at the magic angle (B).

$$S(\phi, z) = \cos\theta \int_{-\infty}^{z} d\xi \xi F(\xi) - \rho \sin\theta \sin\phi\, zF(z) + \frac{\rho^2}{4} \cos\theta \cos 2\phi\, F(z). \quad [3]$$

While the boundary method can produce acceptable coil designs, some amount of iteration is necessary since the *currents are being truncated rather than the magnetic field.* A more direct approach will start from a truncated magnetic field profile, but this presents difficulties when attempting to obtain consistent field profiles that satisfy Maxwell's equations. For this reason, Turner's target field method (*6*) offers an important alternative route to the design of gradient coils. For NMR applications, the component of the gradient field that is parallel to the main polarizing field contributes to the evolution of the NMR signal, and the target field method is simple to implement for coils wound on cylinders coaxial with the polarizing field, as only the z component of the gradient field requires consideration. This allows the target field function to be chosen freely so long as the current density remains finite. For other cylinder orientations, all three components of the gradient field can have nonzero projections along the main polarizing field. However, since currents derived from the boundary method will not depend on the radial component, B_ρ, the target field approach can also neglect this component when choosing a consistent model gradient profile. Consistency for the z and ϕ components can then be ensured by requiring that the relation

$$B_z^{(m)} = -i\left(\frac{\rho}{m}\right) \frac{d}{dz} B_\phi^{(m)} \quad [4]$$

hold for each Fourier component, m, in the Fourier–Bessel series expansion of the magnetic fields. For MAS magic angle gradient applications, this consistency relation puts an acceptable target field in the form

$$B_z = \cos\theta\, zF(z) - \rho \sin\theta \sin\phi \frac{d}{dz}(zF(z)) + \frac{\rho^2}{4} \cos\theta \cos 2\phi \frac{d}{dz} F(z)$$

$$B_\phi = zF(z)\sin\theta \cos\phi - \rho \cos\theta \sin\phi F(z), \quad [5]$$

where $F(z)$ is a suitable truncation function. Truncation of the magnetic field produces a new term in B_z that varies as $\cos 2\phi$ and requires that the z dependence of the $\sin\phi$ term be given by the derivative of the ϕ independent term. These changes in the form of the gradient field will reintroduce modulation from sample spinning. This is basically the effect of having the return paths for the current in proximity to the active volume of the gradient coil. After Fourier transformation to k space, the Fourier components $B_z^{(m)}$ can be used to determine the azimuthal current densities via the standard formula (*6*),

$$J_\phi^{(m)}(k) = e^{-\alpha k^2} \frac{B_z^{(m)}(c, k)}{\mu_0 k I_m(kc) K_m'(ka)}, \quad [6]$$

where a Gaussian apodization factor has been added to ensure finite solutions, and a and c denote the current winding radius and target field radius.

The projection of the gradient magnetic field can then be easily calculated as

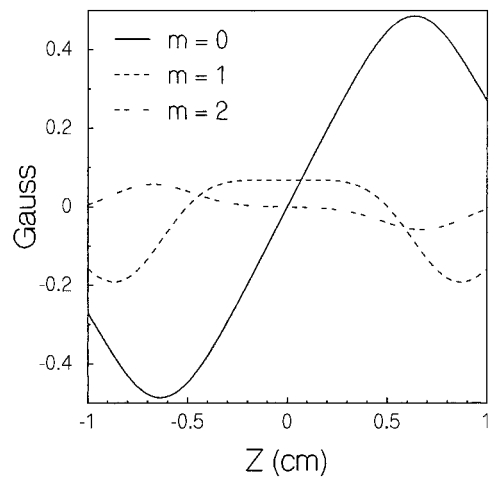

FIG. 2. Magnetic field profiles at a radius of 0.16 cm for the zero-, first-, and second-order harmonics for a MAS magic angle gradient coil with target value of 1 G/cm-A. The first- and second-order harmonics are scaled up by a factor of 10.

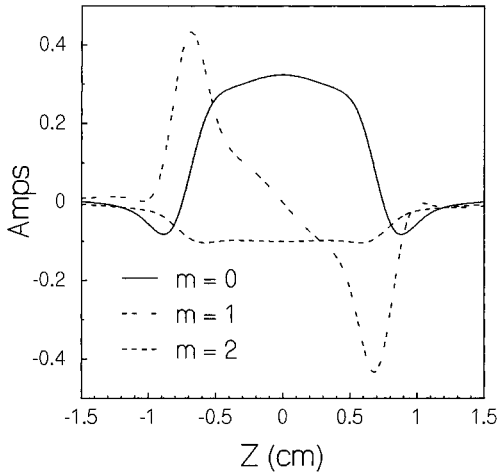

FIG. 3. Integrated current density profiles for the zero-, first-, and second-order harmonics. All curves are scaled identically for a 1 G/cm gradient. The total current is 1.75 A.

$$B_z^{(m)}(k)\cos\theta - B_y^{(m)}(k)\sin\theta = \frac{\mu_0 a}{2\pi} kI_m(k\rho)\Big(-\cos\theta\, J_\phi^{(m)}K'_m(ka) + \frac{1}{2}\sin\theta\,(-J_\phi^{(m-1)}(k)\,K'_{m-1}(ka) + J_\phi^{(m+1)}(k)\,K'_{m+1}(ka))\Big) \quad [7]$$

and after transforming back to z space, the total field can be constructed from

$$B(z) = B^{(0)} + 2iB^{(1)}\sin\phi + 2B^{(2)}\cos 2\phi. \quad [8]$$

One interesting choice for a truncation function is the equiripple profile based on Chebychev polynomials (*8*). This is because the rippled profile can be smoothed considerably by the Gaussian apodization used to guarantee finite current densities, resulting in useful gradient profiles that cover a broader range of coil former geometries. The field profiles obtained by using Eq. [7] for such a design is shown in Fig. 2. For this design, a coil radius of 0.7 cm and a target radius of 0.25 cm was used. A scaling length of $d = 0.4$ was used in the sixth-order Chebychev truncation function,

$$F(z) := \frac{z}{1 + \frac{1}{1000}\,T_3^2(z/d)}, \quad [9]$$

where $T_3(x) = x(4x^2 - 3)$. A small amount of apodization with $\alpha = 0.01$ was used to keep the current densities from diverging for large k. The construction of an actual coil based on the derived current densities requires approximating the continuous current distribution with a finite number of windings. This is accomplished by placing wires along the appropriate contours of the total current distribution, obtained by integrating the current densities, $J_\varphi^{(m)}$, along the length of the cylinder and combining them in the same way as for the magnetic field in Eq. [8]. The curves for the integrated current densities, $S^{(m)}$, are illustrated in Fig. 3. These currents are for a gradient strength of 1 G/cm, and when combined to produce the total current distribution, show that 1.79 A is required. Since an integral number of wire loops are needed in any real coil, the current can be scaled appropriately. The contours, placed at half-odd integer values for a 10-A total winding pattern

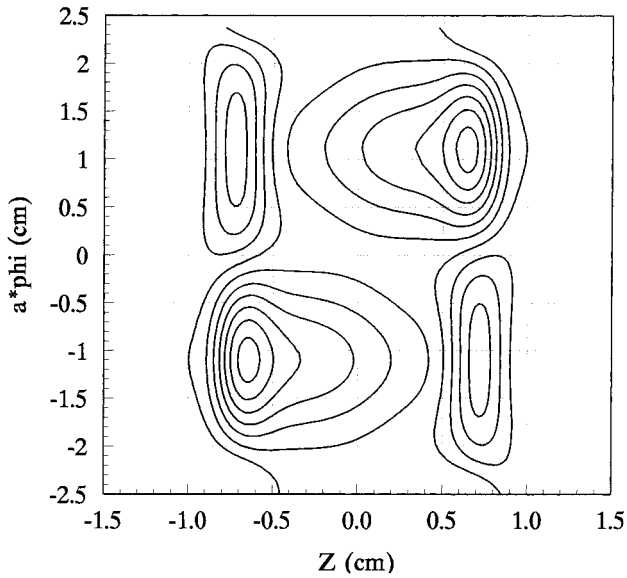

FIG. 4. Contours for a 10-turn coil design resulting in a 5.8 G/cm-A gradient coil. The vertical axis is in units of arc length for the 1.4-cm-diameter coil former.

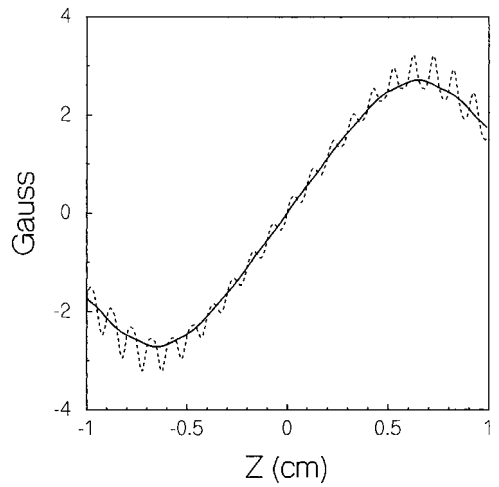

FIG. 5. Magnetic field profiles for the 10-turn coil illustrated in Fig. 4. The field is plotted for a helical trajectory (20 turns) at a radius of 0.01 (solid) and 0.16 cm (dashed).

corresponding to a 5.8 G/cm-A gradient are given in Fig. 4. The actual gradient performance for the discrete winding pattern will differ from that expected from the continuous distribution as calculated from Eq. [7] and displayed in Fig. 2. A graph of the gradient field for a spiral trajectory on and off axis, as calculated for the wire pattern, is given in Fig. 5. In this case, the magnetic field was calculated by approximating the curves with short wire segments and using the standard formulas for finite wire segments. The axial curve very closely fits that obtained via the continuous current distribution. Off the axis, however, the 0.2-G amplitude of the modulation components at the coil center is about 2.5 times larger than that expected from Fig. 2. Since the target method includes the effects of the return current pathways, this is apparently a result of the passage from continuous currents to discrete loops. The extension of the target method presented here can also be used to design efficient gradient coils for sample geometries using horizontal solenoid RF coils, and by adding an additional current layer, the gradient coils can be designed for shielding the exterior field while preserving the interior field gradient linearity.

REFERENCES

1. D. L. Mattiello, W. S. Warren, L. Mueller, and B. T. Farmer, Minimizing the water resonance in biological NMR: Characterization and suppression of intermolecular dipolar interactions by multiple axis gradients, *J. Am. Chem. Soc.* **118,** 3253 (1996).
2. T. M. Barbara, Cylindrical demagnetization fields and microprobe design in high resolution NMR, *J. Magn. Reson. A* **109,** 265 (1994).
3. P. A. Keiffer, The influence of resin structure, tether length, and solvent upon the high resolution ^{1}H NMR spectra of solid phase synthesis resins, *J. Org. Chem.* **61,** 1558 (1996).
4. R. Bowtell and A. Peters, Magic angle gradient coil design, *J. Magn. Reson. A* **115,** 55 (1994).
5. W. E. Maas, F. H. Laukien, and D. G. Cory, Gradient, high resolution, magic angle sample spinning NMR, *J. Am. Chem. Soc.* **118,** 13085 (1996).
6. R. Turner, A target field approach to optimal coil design, *J. Phys. D* **19,** L147 (1986).
7. B. H. Suits and D. E. Wilken, Improving magnetic gradient coils for NMR imaging, *J. Phy. E.* **22,** 565 (1989).
8. M. C. Leifer, RF solenoid with extended equiripple field profile, *J. Magn. Reson. A* **105,** 1 (1993).